Kazumi KURIHARA, Tomotsugu KUBOTA, Daisuke NITAWAKI

Ibaraki University

Rotor Design for High Starting Performance of a Self-Starting Single-Phase Permanent-Magnet Motor

Abstract. *This paper presents a rotor design for high starting performance of a line-start single-phase permanent-magnet motor. Two-dimensional time-stepping finite-analysis has been used to successfully predict the starting performance of the proposed motor with the new rotor configuration. The comparison of the starting performance between experimental and proposed motors was done. It was found from the simulation and experimental results that the proposed motor has the excellent synchronous pull-in characteristic under rated torque.*

Streszczenie. *W pracy przedstawiono projekt wirnika szybko startującego jednofazowego silnika z ze startem liniowym. Zastosowano w tym celu analizę elementowo-skończeniową. Przeprowadzono porównanie początkowego działania dwóch urządzeń, Odkryto podczas symulacji komputerowej, że proponowany silnik posiada doskonałą charakterystykę. (**Projekt wirnika szybko startującego jednofazowego z magnesami trwałymi**)*

Keywords: single-phase permanent-magnet motor, high starting performance, time-stepping finite-element analysis, high-efficiency.
Słowa kluczowe: projekt wirnika szybko startującego jednofazowego, szybko startujące działanie, analiza elementowo-skończeniowa w dziedzinie czasu, wysoka efektywność.

Introduction

Self-starting single-phase permanent-magnet (PM) motors [1, 2] are suited for application in home appliances, such as refrigerator compressors. In the single-phase motors, where the auxiliary winding is supplied through a capacitor, the operation has been complicated by the imbalance between the main and auxiliary winding voltages. In particular, the negative sequence field causes the negative average torque as well as the PMs at asynchronous speed. Because of this, the pull-in torque of the single-phase capacitor-start PM motor is lower than that of a self-starting three-phase PM motor. Therefore, the optimal design to improve the pull-in torque has been needed.

This paper presents a rotor design of the line-start single-phase PM motor which has the excellent pull-in characteristic. The rotor configuration of the proposed motor and the line-starting performance are shown. A comparison of starting performance between experimental and proposed motors was done. It was found from the simulation and experimental results that the proposed motor has the excellent synchronous pull-in characteristic under rated torque and that the synchronous performance is the same as that of the experimental motor.

Method for Analysis

The analysis for taking the eddy currents into account, in general, becomes essential to solve the three-dimensional problem. In this paper, it is assumed that the eddy currents flow approximately in the axial direction, because the experimental rotor is equipped with end rings. This reduces the analysis to a two-dimensional problem. The effect of the eddy current for the rotor ends is taken into account by multiplying the conductivity of the rotor bars by the coefficient [3]. The fundamental equations for the magnetic field are represented in the two-dimensional rectangular co-ordinates as

$$\frac{\partial}{\partial x}\left(\nu\,\frac{\partial A}{\partial x}\right)+\frac{\partial}{\partial y}\left(\nu\,\frac{\partial A}{\partial y}\right)=-J_0-J_e-J_m \tag{1}$$

$$J_e=-\sigma\frac{\partial A}{\partial t} \tag{2}$$

$$J_m=\nu_0\left(\frac{\partial M_y}{\partial x}-\frac{\partial M_x}{\partial y}\right) \tag{3}$$

where: A– z-component of magnetic vector potential $\boldsymbol{A}$, J_0 – stator-winding current density, J_e – eddy current density, J_m – equivalent magnetizing current density, M_x, M_y– x and y components of the magnetization $\boldsymbol{M}$, respectively [4], σ – conductivity, ν – reluctivity.

The value of ν in the PM is assumed the same as the reluctivity of free space ν_0. J_m is assumed zero outside the PM.

The effect of the eddy current for the rotor ends is taken into account by multiplying by the coefficient k_c as described below. It is done to reduce the analysis to two dimensional. The equivalent resistance R_2 for the rotor bars including the rotor end rings can be given below if the bars are distributed at equal intervals in the rotor [5].

$$R_2=R_b+R_e\frac{Z_2}{\left(2p\pi\right)^2} \tag{4}$$

where: R_b – resistance of a bar, R_e – resistance of end rings, Z_2 – number of rotor slots, p – pole pair number.

Therefore, k_c [3] is given by

$$k_c=\frac{R_b}{R_2} \tag{5}$$

This coefficient k_c is found effective to take into account the rotor-bar current for the foundamental space harmonic. Moreover, it has been found that the agreement between computed and measured results of the starting performance characteristics in the experimental motor is good [1]. Therefore, it is considered that design use of the k_c is acceptable, even if the higher space harmonics exists [6].

Fig. 1 shows the circuit of the experimental motor [1]. The voltage and current equations are given as

$$e_m+r_m i_m+L_m\frac{\partial i_m}{\partial t}=v \tag{6}$$

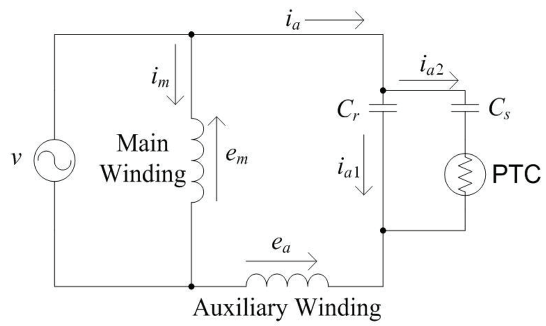

Fig. 1. Circuit of a single-phase capacitor-run PM motor

(7) $$e_a + R_a i_a + L_a \frac{\partial i_a}{\partial t} + \frac{1}{C_r}\int i_{a1} dt = v$$

(8) $$i_a = i_{a1} + i_{a2}$$

(9) $$\frac{1}{C_r} i_{a1} = \frac{1}{C_s} i_{a2} + r_s \frac{\partial i_{a2}}{\partial t}$$

where: v–terminal voltage, r_m– resistance of main winding, L_m –end-winding leakage inductance of main winding, r_a– resistance of the auxiliary winding, L_a – end-winding leakage inductance of auxiliary winding, r_s – resistance of PTC.

e_m is given by the line integral of the vector potential round c_m which is along the main winding, similarly, e_a is given by the line integral of the vector potential round c_a which is along the auxiliary winding. i.e.,

e_a is given by the line integral of the vector potential round c_a which is along the stator windings of phase *a* [2]

(10) $$e_m = \oint_{c_m} \frac{\partial A^t}{\partial t} ds = \sum_{k=1}^{N} \left(\oint_{c_m{}^{(k)}} \frac{A^{t(k)} - A^{t-\Delta t(k)}}{\Delta t} ds \right)$$

(11) $$e_a = \oint_{c_a} \frac{\partial A^t}{\partial t} ds = \sum_{k=1}^{N} \left(\oint_{c_a{}^{(k)}} \frac{A^{t(k)} - A^{t-\Delta t(k)}}{\Delta t} ds \right)$$

where: A^t – A at time t, Δt– time step, N– is number of slices.

$c_m{}^{(k)}$ and $c_a{}^{(k)}$ are the vector potential rounds of the kth slice, respectively [1].

The dynamic equation is given as [7]

(12) $$T = J\frac{d\omega_r}{dt} + B_0 \omega_r + T_l$$

where: B_0– friction coefficient, T_l– load torque.

$T^{(k)}$ in the kth slice is calculated by using the *Bil* rule [8].

(13) $$T = \sum_{k=1}^{N} T^{(k)}.$$

ω_r is given by

(14) $$\omega_r = \frac{d\theta}{dt}.$$

One obtains the following equation by substituting (14) in (12):

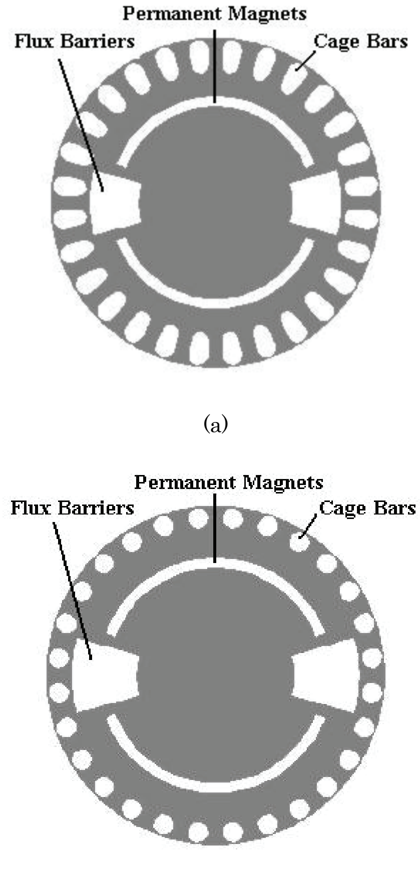

(b)

Fig. 2. Cross section (a) Experimental (prototype) rotor (b) Proposed rotor

(15) $$T = J\frac{d^2\theta}{dt^2} + B_0 \frac{d\theta}{dt} + T_l.$$

In this paper, the forward difference method is used to obtain the rotational angle at time t because the vector potential, currents and rotational angle at time t- Δt are all known.

We have

(16) $$\frac{d\theta^{t-\Delta t}}{dt} = \frac{\theta^t - \theta^{t-\Delta t}}{\Delta t}$$

(17) $$\frac{d^2\theta^{t-\Delta t}}{dt^2} = \frac{\theta^t - 2\theta^{t-\Delta t} + \theta^{t-2\Delta t}}{(\Delta t)^2}.$$

One obtains the following equation by substituting (16) and (17) in (15) [7]:

(18) $$\theta^t = \frac{1}{J + B_0\Delta t}[(T^{t-\Delta t} - T_l^{t-\Delta t})(\Delta t)^2 + (2J + B_0\Delta t)\theta^{t-\Delta t} - J\theta^{t-2\Delta t}].$$

In the case when the effect of the friction is negligibly small, (18) can be represented simply as follows:

(19) $$\theta^t = \frac{(\Delta t)^2}{J}\left(T^{t-\Delta t} - T_l^{t-\Delta t}\right) + 2\theta^{t-\Delta t} - \theta^{t-2\Delta t}.$$

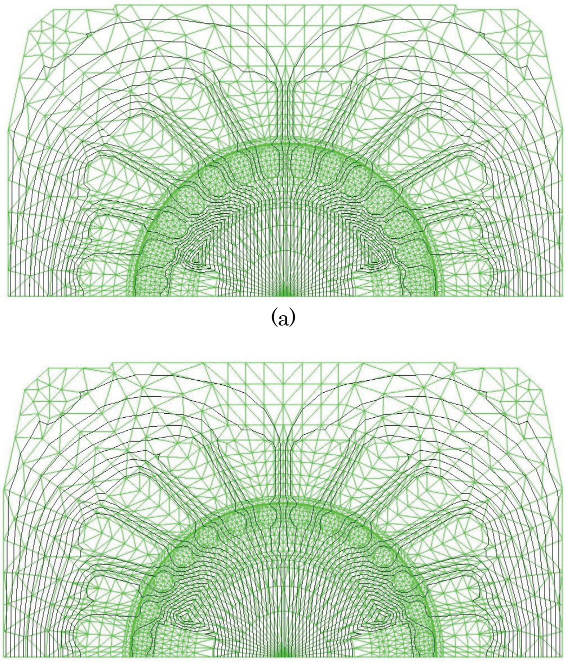

(a)

(b)

Fig. 3. Flux distribution caused by PMs (a) Experimental Motor (b) Proposed Motor

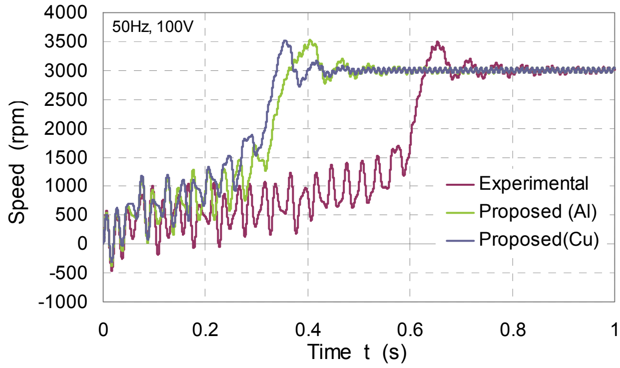

Fig. 4. Computed results of speed-time responses

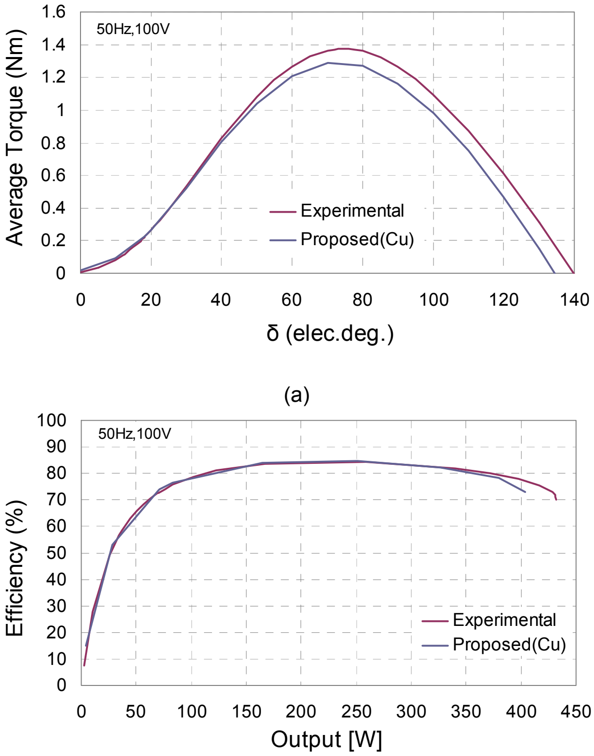

(a)

(b)

Fig. 5. Computed results of load performance characteristics (a) Average torque versus load angle δ. (b) Efficiency versus output

One can obtain the vector potential, currents and rotational angle by solving (1), (6)-(9), and (15) using the time-stepping finite element technique [1].

Steady-state synchronous and transient performance

In this paper, a 50Hz, 100V two-pole single-phase capacitor-start squirrel-cage induction motor [1] was used for testing the experiment and proposed motors. The rated torque and output power are 0.225 Nm and 70.7 W, respectively. The stack length of the stator was 32.0mm. The starting capacitor is 150 μF and the running capacitor is 14 μF.

Fig.2 shows the cross sections of the experimental and proposed rotors, respectively.

Oxygen-free copper (Cu) and pure aluminum (Al) is chosen as the rotor-bar material of the proposed motor, respectively. Really, the rotor with the oxygen-free copper bars was built. The rotor-bar configuration and positions of the PMs are designed from the simulation results of the steady and transient performance analysis by using the time-stepping finite-element technique [1]. Of course, the configuration of flux barriers has been changed for reducing the leakage flux in the rotor. Furthermore, the configuration and dimensions of the rotor with oxygen-free copper are the same as those of the rotor with pure aluminum. The material of the end ring is also the same as that of the rotor bar. However, the length of the end ring is changed to keep the value of R_2 of (4) constant.

Fig. 3 shows the flux distribution of the experimental and proposed motors caused by PMs.

Fig. 4 shows the computed results of the speed-time responses for the experimental and proposed motors under a constant rated torque, respectively. It was found from Fig. 4 that the proposed motor has the excellent synchronous pull-in characteristic.

Fig. 5 shows the computed results of the load performance characteristics. It can be seen from Fig. 5 (a) that the maximum torque decreases slightly, however the load angle δ at rated torque is the same as that of the experimental motor. It was found from Fig. 5 (b) that the efficiency at rated output increases slightly. On the other hand, it is clear that the starting performance capability is largely improved as described above.

Experimental results

In the experiment, the applied voltage v is given as by using phase angle ϕ_1.

$$v = \sqrt{2}V_l \sin\left(\omega t + \phi_1\right) \tag{20}$$

where: V_l – rms of terminal voltage, ω –angular frequency.

Fig. 6 and Fig.7 show the photograph of the proposed rotor and the experimental setup, respectively.

Fig. 8 shows the experimental results of the speed versus time responses when ϕ_1=180° from no load to 140% of rated torque.

We confirmed by using the proposed rotor that the start-up and synchronous pull-in characteristics are realized at 130% value of the rated load torque.

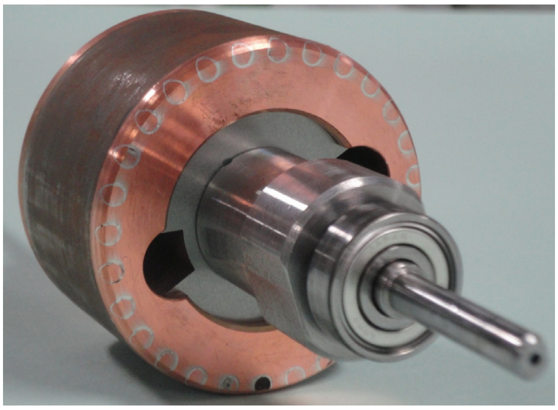

Fig. 6. Proposed rotor

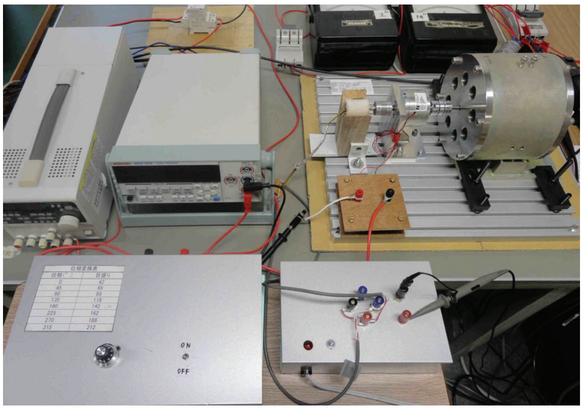

Fig. 7. Experimental setup.

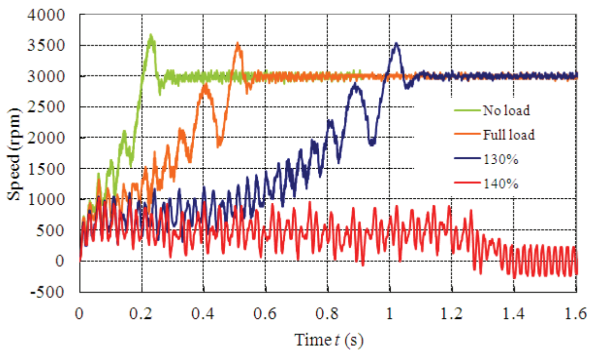

Fig.8. Experimental results of speed versus time responses.

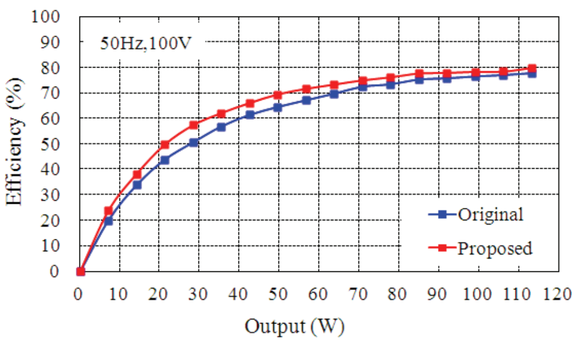

Fig. 9. Experimental results of efficiency versus output

Fig. 9 shows the experimental results of the efficiency versus output powers at 100V. It can be seen that the efficiency of the proposed motor is higher than that of the experimental (original) motor. The efficiency of the proposed motor at rated output was 75.1% and 2.5% higher than that of original motor.

Conclusion

A successful rotor design for high starting performance of a line-start single-phase PM motor was developed. The configuration and dimensions of the rotor were determined from the simulation results, where time-stepping finite-element analysis has been used to successfully predict the dynamic and transient performance of the proposed motor. It was found from the simulation and experimental results that the proposed motor has the excellent synchronous pull-in characteristic under rated torque and that the synchronous performance is the same as that of the experimental motor.

REFERENCES

[1] Hori M., Kurihara K., Kubota T., Starting performance analysis for a single-phase capacitor-run permanent magnet motor with skewed rotor slots, in *Proc. Int. Conf. Elect. Machines*, Vilamoura, Portugal, Sept. 6-9, (2008)

[2] Kurihara K., Imaizumi Y., Kubota T., Torque ripple minimization of a single-phase capacitor-run permanent-magnet motor using response surface methodology, in *Proc. Int. Symposium Electromagnetic Fields*, Arras, France, Sept. 10-12, (2009)

[3] Kurihara K., Rahman M. A., High-efficiency line-start interior permanent-magnet synchronous motors, *IEEE Trans. Ind. Applicat.* 40 (2004), No.3, 789-796

[4] Nakata T., Takahashi N., *Finite Element Method in Electrical Engineering*, Tokyo Japan: Morikita, (1982)

[5] Takeuchi J., *Design of Electrical Machines*. Tokyo, Japan: Ohmsha, (1993)

[6] Kurihara K., Wakui G., Kubota T., Steady-state performance analysis of permanent magnet synchronous motors including space harmonics, *IEEE Trans. Magn.*, 30 (1994), 1306-1315

[7] Kurihara K., Wakui G., Kubota T., Transient performance analysis of permanent magnet synchronous motors, *Trans. Inst. Elect. Eng. Jpn,* 114-D (1994), No.5, 551-560

[8] Binns K.J., Riley C.P., Wong M., The efficient evaluation of torque and field gradient in permanent-magnet machines with small air-gap, *IEEE Trans. Magn.* 21 (1985), 2435-2438

***Authors**: Prof. Kazumi Kurihara, Ibaraki University, Hitachi 316-*8511, Japan, E-mail: kurihara@mx.ibaraki.ac.jp; Tomotsugu Kubota, Ibaraki University, Hitachi 316-8511, Japan, E-mail: kubota@mx.ibaraki.ac.jp*; Daisuke Nitawaki, Ibaraki University, Hitachi 316-8511, Japan.*

The correspondence address is:
e-mail: kurihara@mx.ibaraki.ac.jp